Lab on a Chip

Label-free Electrochemical Immunosensor based on Decorated Cellulose Nanofibrous Membrane for Point-of-Care Diagnosis of Amanitin Poisoning via Human Urine

Journal:	*Lab on a Chip*
Manuscript ID	LC-ART-06-2023-000508.R1
Article Type:	Paper
Date Submitted by the Author:	29-Aug-2023
Complete List of Authors:	El-Moghazy, Ahmed; University of California Davis, ; City of Scientific Research and Technological Applications, Amaly, Noha; University of California Davis; City of Scientific Research and Technological Applications, Nitin, Nitin; University of California Davis Sun, Gang; University of California Davis

SCHOLARONE™
Manuscripts

1
2
3   **Label-free Electrochemical Immunosensor based on Decorated Cellulose Nanofibrous**
4   **Membrane for Point-of-Care Diagnosis of Amanitin Poisoning *via* Human Urine**
5

6   Ahmed Y. El-Moghazy [1,2] *, Noha Amaly [1,2], Nitin Nitin [1,3], Gang Sun [1]
7

8   [1] *Department of Biological and Agricultural Engineering, University of California, Davis, CA 95616,*
9   *USA.*
10   [2] *Polymeric Materials Research Department, Advanced Technology and New Materials Research*
11   *Institute, City of Scientific Research and Technological Applications (SRTA-City), New Borg El-Arab City*
12   *21934, Alexandria, Egypt.*
13   [3] *Food Science and Technology, University of California, Davis, United States.*

14
15

16   **Abstract:**

17

18   α-Amanitin (AMN) is one of the deadliest toxins from mushrooms, present in the deadly

19   mushroom species *Amanita phalloides*. It is a bicyclic octapeptide and represents up to 40% of the

20   amatoxins in mushrooms, damaging the livers and kidneys. Current methods of detecting

21   amatoxins are time-consuming and require use of expensive equipment. A novel label-free

22   electrochemical immunosensor was successfully developed for rapid detection of α-amanitin,

23   which was fabricated by immobilization of anti-α-amanitin antibodies onto functionalized

24   cellulose nanofibrous membrane-modified carbon screen-printed electrode. An oxidation peak of

25   the captured amanitin on the tethered antibodies was observed at 0.45 V. The performance of the

26   nanofibrous membrane on the electrode and necessary fabrication steps were investigated by

27   electrochemical impedance spectroscopy (EIS) and cyclic voltammetry (CV). Due to their unique

28   structural features and properties such as high specific surface areas and microporous structure,

29   the nanofibrous membrane as the immunosensor matrix for the antibody tethering exhibited

30   improved electrochemical performance of the electrode by more than 3 times compared with the

31   casted membranes. Under the optimal conditions, the assembled immunosensor exhibited high

32   sensitivity toward α-amanitin detection in the range of 0.009-2 ng mL^{-1} with a limit of detection

33   of 8.3 pg mL^{-1}. The results clearly indicate that the fabricated nanofibers-based-immunosensor is

34   suitable to point-of-care detection of lethal α-amanitin in human urine without any pretreatment

35   within 30 min.

36   **Keywords:** α-amanitin, Cellulose, Nanofibers, Electrochemical immunosensor, Point-of-care.

37

Introduction:

39   Thousands of mushroom poisonings are reported annually around the globe [1–3]. In over 80% of

40   cases of mushroom poisoning, the kind of mushroom is unknown. Based on the poisons present

41   and the clinical symptoms they cause, toxic mushrooms are frequently categorized [5]. Amatoxins

42   are one of the most toxic groups of mushroom toxins, and are responsible for the majority of fatal

43   mushroom poisonings worldwide. These toxins are produced by several species of mushrooms,

44   including some of the Amanita genus, such as Amanita phalloides, also known as the death cap

45   mushroom, which is responsible for most mushroom poisoning deaths [4].

46   Amatoxins are highly stable and heat-resistant, which means that they are not destroyed by cooking

47   or processing. Once ingested, they are absorbed rapidly in the small intestine and transported to

48   the liver, where they bind to RNA polymerase II, a critical enzyme involved in protein synthesis.

49   This results in the inhibition of protein synthesis, leading to liver cell death and liver failure [5].

50   The symptoms of amatoxin poisoning usually appear within 6 to 24 hours after ingestion, and may

51   include gastrointestinal distress (such as nausea, vomiting, and diarrhea), abdominal pain, and

52   dehydration. These symptoms may improve after a few days, but then the patient may develop

53   severe liver damage, which can lead to hepatic encephalopathy, coma, and death. Treatment of

54   amatoxin poisoning often involves supportive care, such as fluid and electrolyte replacement, and

55   sometimes liver transplantation is necessary [6].

56   The diagnosis of amatoxin poisoning can be challenging, as symptoms may not appear until several

57   hours after ingestion, and may initially resemble a gastrointestinal illness. Currently, there are no

58   rapid or on-site diagnostic tools for amatoxin poisoning, which can delay the diagnosis of

59   poisoning and subsequent treatment [7].

60   Laboratory-based analysis is typically required, using techniques such as HPLC, mass

61   spectrometry, or ELISA to detect the presence of amatoxins in blood, urine, or mushroom extracts

62   [7,8]. The diagnosis of amatoxin poisoning is usually based on a combination of clinical symptoms,

63   history of mushroom ingestion, and laboratory results. In patients with suspected amatoxin

64   poisoning, treatment should be initiated immediately based on clinical suspicion, even before

65   laboratory results are available [7–9].

66   Rapid diagnosis of amatoxin poisoning would allow for prompt initiation of appropriate treatment,

67   including the administration of silibinin, which can improve patient outcomes and potentially

68   reduce the need for more invasive treatments such as liver transplantation [9,10]. The development

69   of biosensors for amatoxins is urgently needed to help for the rapid and on-site diagnosis of

70   amatoxin poisoning, which allowing for quick and easy detection of amatoxins in mushroom

71   samples or biological samples from patients with suspected poisoning.

72   In the recent years, nanomaterials have opened new horizons for the biosensor development with

73   enhanced sensitivity, selectivity, and shortened detection time due to the ultrahigh surface areas

74   [11–15]. Nanofibers (NFs) produced by electrospinning are among the most promising nanomaterials,

75   gained a growing interest during the past decade for a wide range of applications [16–20].The

76   employment of nanofibers with ultrahigh surface area has resulted in sensors with higher

77   sensitivity and lower limits of detection (LOD) [21,22].

78   In this study, an ultrasensitive label-free electrochemical immunosensor was developed based on

79   citric acid decorated cellulose nanofibrous membranes immobilized with AMN antibodies to rapid

80   detection of AMN in human fluids samples. The membrane is attached onto printed electrodes.

81   Amperometric responses were based on the oxidation of hydroxyindole of the captured AMN

82   molecules on the surface of anti-AMN-modified screen-printed electrodes. The developed label-

83   free electrochemical immunosensor was applied for AMN detection in real human urine samples.

84

85   **Materials & Methods**

86   ***Chemicals, Materials, and Instrument.***

87   Cellulose acetate (CA; white powder; Mw = 30,000 Da), N, N-dimethylacetamide (DMAc), citric

88   acid, α-Amanitin were purchased from Sigma (St. Louis, MO). N-Ethyl-N'-(3- dimethyl

89   aminopropyl) carbodiimide hydrochloride (EDC), N-hydroxyl succinimide (NHS), disodium

90   hydrogen phosphate (Na_2HPO_4), and monosodium orthophosphate (NaH_2PO_4) were supplied by

91   Acros Chemical (Pittsburgh, PA, USA). sodium chloride (NaCl), potassium chloride (KCl), bovine

92   serum albumin (BSA), potassium ferricyanide ($K_3[Fe(CN_6)]$), potassium ferrocyanide

93   ($K_2[Fe(CN_6)]$) were purchased from Sigma-Aldrich (Milwaukee, WI, USA), AMN antibody (anti-

94   AMN) was generously donated by Dr. Candace Bever (USDA-ARS). All water used was purified

95   using a Millipore Milli-Q plus water purification system. All chemicals were used as received.

96   A 263A potentiostat/galvanostat equipped with a frequency response detector (FRD100)

97   (Princeton Applied Research Co., Oak Ridge, TN, USA) was used for the electrochemical

98   measurements. The disposable SPE, comprising a carbon working electrode, a carbon counter

99   electrode, and an Ag/AgCl reference electrode, was purchased from Metrohm USA INC (GA, US).

100 The morphological characterizations of the polymeric nanofibrous membranes were implemented

101 by a FEI 430 Nova NanoSEM scanning electron microscope (SEM).

102 The FT-IR spectra of membrane materials were achieved by using a Nicolet 6700 spectrometer,

103 following of the pressing of the grounded the Cel-A/Cel NFMs at the different reaction steps with

104 anhydrous KBr, FT-IR spectra of these specimens were scanned in the wavenumber range of 500-

105 4000 cm^{-1} with a resolution of 4 cm^{-1}.

106

107 ***Cellulose nanofibrous membranes production and functionalization:***

108 *Cellulose acetate nanofibrous membranes production*

109 Following Fu et al [23]. with minor modifications, cellulose acetate nanofibrous membranes (Cel-A

110 NFMs) were produced through electrospinning. Cellulose acetate was dissolved with vigorous

111 stirring overnight in a solvent combination of DMAC and acetone (1:1 w/w), and solutions of

112 various concentrations (5, 10 and 15 wt%) were prepared. A 10-mL plastic syringe with an 18-

113 gauge tubular metal needle with a flat tip was used for the electrospinning process, which was

114 carried out using a DXES-1 spinning apparatus at a voltage of 20 kV, a distance of 15 cm between

115 the needle tip and the collector surface, and a feeding rate of 1 mL/h for the delivery of the

116 polymeric solution. The spinning process was performed at room temperature and humidity of 45

117 ± 5%.

118

119 *Deacetylation of cellulose acetate nanofibrous membranes*

120 Cellulose nanofibrous membranes (Cel NFMs) were made by deacetylating Cel-A NFMs. To

121 hydrolyze the acetate groups and create Cel NFMs, the deacetylation procedure was carried out in

122 0.05 M NaOH in 1:1 EtOH/water solutions at room temperature for 48 hours. After rinsing with

123   ultrapure water, the prepared Cel NFMs were dried in a vacuum oven for 12 hours at 80 °C. The

124   acetyl% of the produced cellulose was determined by immersing a membrane sample in 20 mL of

125   0.05 N NaOH in 50% ethanol for 12 hours at room temperature. Followed by titrating of excess

126   alkali with 0.05 N HCl using a pH meter. The percentage of acetyl % in cellulose was calculated

127   according to equation (1) [24]:

128                            $\text{Acetyl } \% = (V_B \cdot C_B - V_A \cdot C_A)\, 4.3/W$ (1)

129   Where W is the sample weight, V_B and C_B are the volume and concentration of NaOH solution,

130   and V_A and C_A are the volume and concentration of HCl solution, respectively.

131

132   *Functionalization of produce nanofibrous membranes*

133   The hydroxyl groups on the Cel NFMs were then reacted with the carboxylic groups of citric acid

134   in a procedure performed as follows [25]: A citric acid solution 8 % (w/v) was prepared in 10 mL of

135   PBS buffer pH 7.2, followed by adding EDC and NHS at a final concentration of 1 mM to the

136   citric acid solution. This mixture was vigorously stirred at room temperature for 2 hours. Then, the

137   Cel NFMs were submerged in the prepared solution for 1 hour at 60 °C. Subsequently, the

138   modified membranes (Cel-CA NFM) were rinsed using PBS and placed in a vacuum oven at 80

139   °C for 1 h.

140   ***AMN Immunosensor fabrication:***

141   *Immobilization of anti-amanitin antibodies*

142   Prior to the sensor fabrication, the screen-printed electrodes will be pretreated by applying

143   potentials between 1 and -1.5 V vs. Ag/AgCl in 0.5 M H_2SO_4 until a stable signal is obtained to

144   remove the organic binders. A 4 mm Cel NFM disc with 0.05 mm thickness was laminated on the

145   working electrode of the SPE using a conductive paste to fabricate Cel NFM/SPE, and similarly

146　Cel casted membranes were used for in parallel preparing of Cel CM/SPE. 100 µL of 1mM

147　EDC/NHS was used to activate the carboxylic groups of the Cel-CA NFMs/SPE for 1 hour. After

148　washing with PBS, 10 µL of anti-AMN (100 µg mL^{-1}) antibodies were dropped onto the surface

149　of EDC/NHS decorated Cel-CA NFMs/SPE, and the electrode was kept at 4°C for 1 hour.

150　Followed by being rinsed with PBS to remove any un-immobilized antibodies, the remaining

151　active groups were blocked with 50 µL of 1% BSA for 1 hour at the room temperature, and then

152　rinsed again with PBS. The resulting immunosensor was then operational for AMN detection

153　experiments. The schematic diagram of the assembly steps of the AMN immunosensor and

154　detection mechanism are illustrated in scheme 1.

155
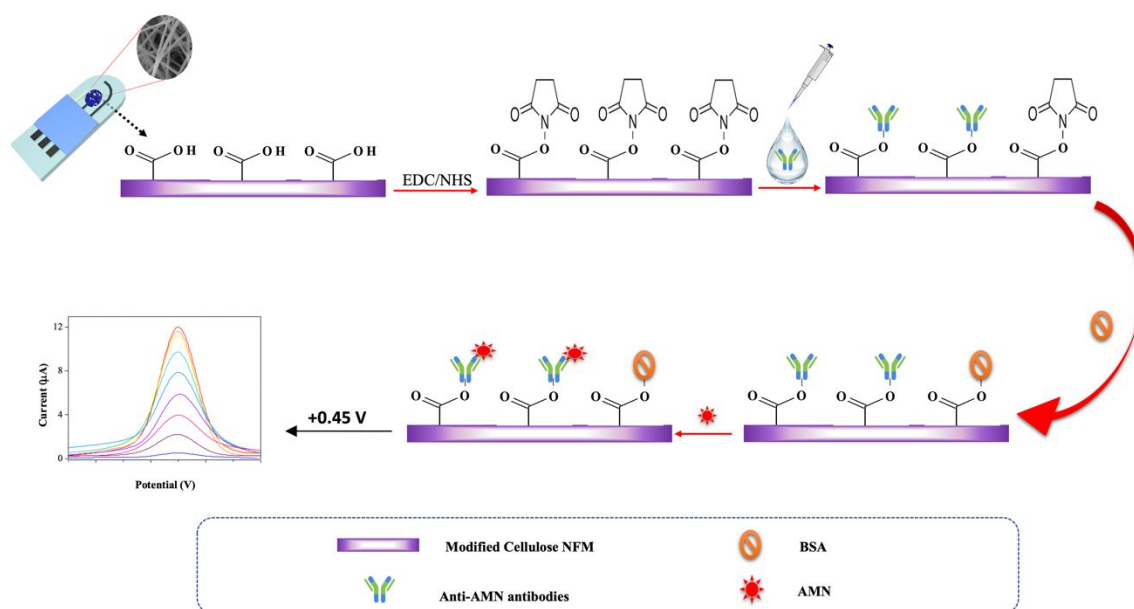
Scheme 1: Fabrication process and sensing mechanism of the electrochemical immunosensor for
AMN detection

158

Electrochemical measurements

160　The electrochemical characterizations for the assembled immunosensor were performed by cyclic

161　voltammetry and Electrochemical impedance spectroscopy (EIS) in a 2.5 mM ferri/ferrocyanide

162　([Fe(CN)$_6$]$^{4-/3-}$) solution. Cyclic voltammograms (CV) were recorded from -1 to 1 V *vs* Ag/AgCl

163   at a scan rate of 25 mV s^{-1}. The Nyquist plots were recorded at applied potential of 0.09 V *vs*

164   Ag/AgCl, with a frequency range from 10 KHz to 1 Hz. Differential pulse voltammetry (DPV)

165   measurements were carried out with applied potential range of 200 – 700 mV, pulse amplitude 60

166   mV, pulse period 200 ms, pulse width 100 ms and scan rate of 50 mV/s. The electrochemical

167   measurements were conducted at least in triplicates using a 263A potentiostat/galvanostat

168   equipped with a frequency response detector (FRD100) (Princeton Applied Research Co., Oak

169   Ridge, TN, USA).

170

171   ***Applicability of the immunosensor for real sample analysis***

172   Urine samples were gathered from a healthful person and spiked with various concentrations of

173   AMN from 0.01 to 1 ng mL^{-1} after the negative AMN content verified using LC-MS. Informed

174   consent was obtained from the participant enrolled in this study. The sample collection and

175   analysis steps followed the IRB-approved protocol (Faculty of Medicine Ethical Committee-

176   Alexandria University, IRB approval No: 00012098) and followed the principles outlined in the

177   Declaration of Helsinki for all human experimental investigations. Prior the direct analysis using

178   the developed immunosensor, the urine samples were diluted 2 times with PBS buffer pH 7.2.

179

180   **Results and discussion**

181
182
183   ***Physico-Chemical characterizations of the produced Cel NFMs***
184

185   First, cellulose nanofibers were created from cellulose acetate nanofibers using a regeneration

186   approach (Fig. 1A). The successful conversion of acetate group of Cel-A to hydroxyl groups of

187   cellulose was proofed using Fourier-transform infrared spectroscopy (FT-IR). Figure 1B presents

188   the FT-IR spectra of the Cel NFM (curve b) and the pristine Cel-A NFM (curve a). After the

189   regeneration process, the peak at around 1750 cm^{-1} ascribed to C=O of the ester of Cel-A

190   disappeared and a new distinctive peak at about 3450 cm^{-1} corresponded to the stretching vibration

191   of -OH appeared (Figure 1B), suggesting that acetate was successfully converted to hydroxyl

192   groups.

193   The decoration of the cellulose nanofibrous membranes with citric acid was carries out as shown

194   in Fig. 1C. The appeared peak of C=O of the ester at 1750 cm confirmed the successful grafting

195   of CA onto the NFM and the effective incorporation of carboxyl groups onto the Cel NFM surface

196   between the hydroxyl group of the regenerated cellulose nanofibers and carboxylic acid (-COOH)

197   group of CA, and the decrease of hydroxyl group peak intensity at 1042 cm^{-1} (Fig. 1D) [26,27].

198

199
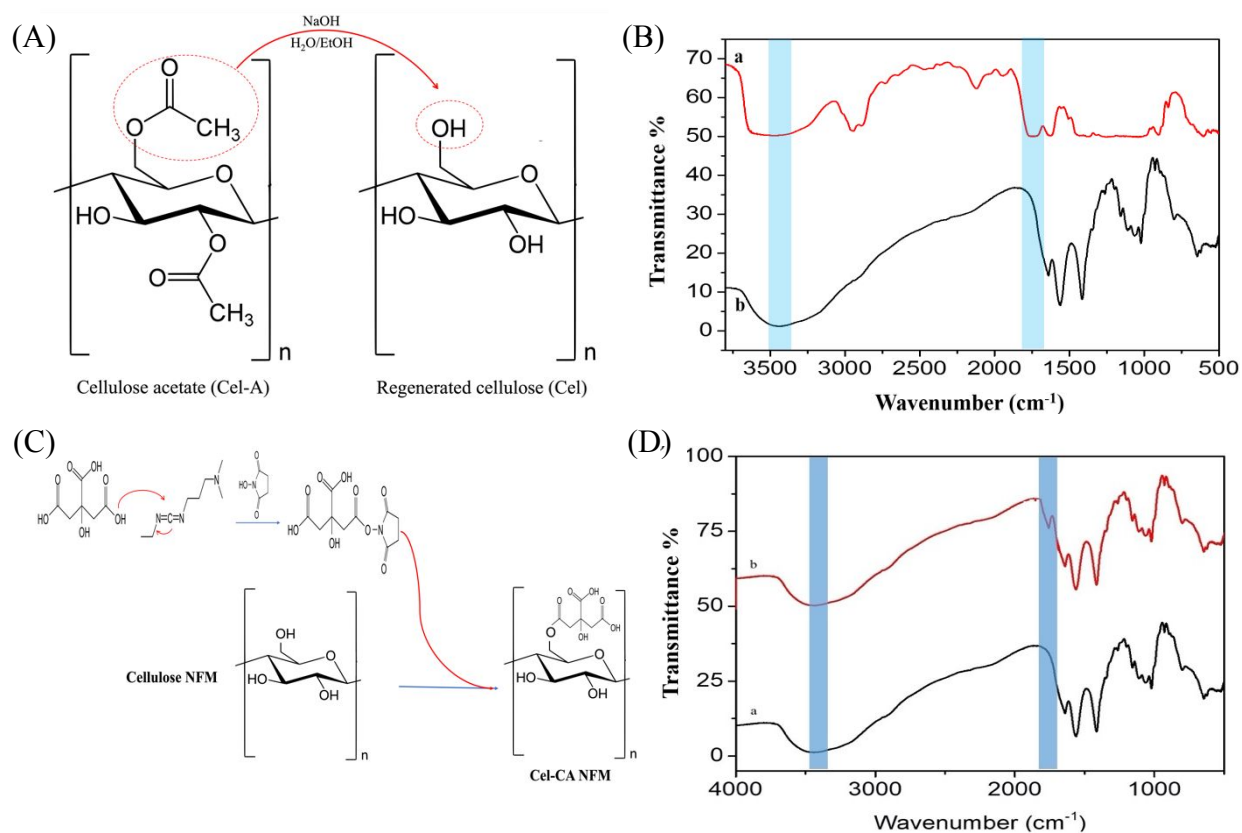
200   Fig.1. (A) Scheme of deacetylation process of cellulose acetate. (B) FT-IR spectra of (a) Cel-A
201   NFM, (b) regenerated Cel NFM. (C) Scheme of grafting of citric acid onto Cel NFM. (D) FT-IR
202   spectra of (a) Cel NFM, (b) Cel NFM decorated with citric acid.
203

204   The morphologies of the nanofibrous membranes were characterized by scanning electron

205   microscopy (SEM). SEM images of electrospun Cel-A NFMs in Fig. 2 a and b demonstrated that

206   the Cel-A nanofibers were aligned and assembled with average diameter of 290 nm as a non-

207   woven fabric [28]. The Cel-A nanofibers ester groups were converted through the deacetylation

208   process to hydroxyl groups, the Cel NFMs still retained the morphology and similar average

209   diameter (Fig. 2 c and d).

210   (a)   (b)

216   (c)   (d)
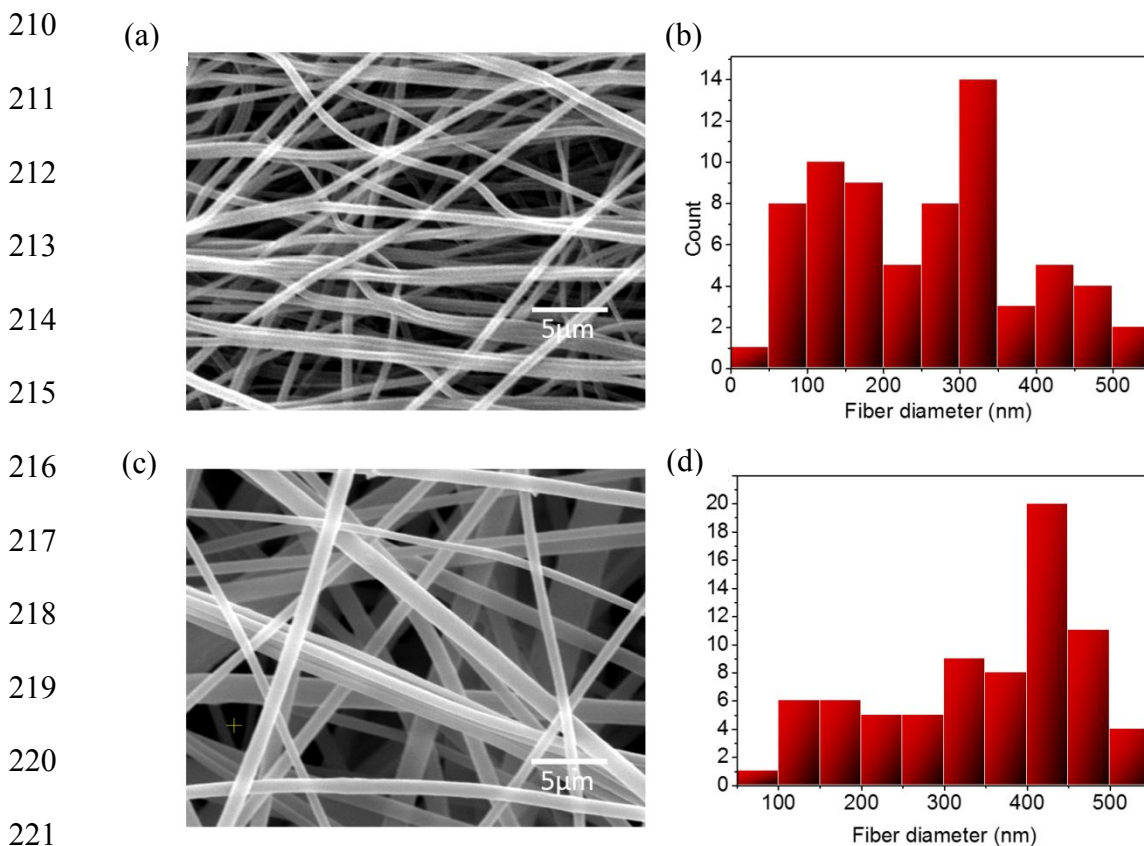
222   Fig. 2. (a) SEM images and (b) diameter distribution of cellulose acetate NFM. (c) SEM images
223   and (d) diameter distribution of Cel NFM.
224
225

226 *Electrochemical impedance spectroscopy and cyclic voltammetry characterization*

227 The effect of using of the nanofibrous membranes as a supporting matrix for the immobilization

228 of the antibodies during the immunosensor fabrication was examined by comparing the

229 electrochemical performance between screen-printed electrodes modified with Cel casted

230 membranes (Cel CM/SPE) and Cel nanofibrous membranes (Cel NFM/SPE). The effective surface

231 area of the different modified electrodes was calculated according to Randles-Sevcik equation [29].

$$i_p = 2.69 \times 10^5 \, An^{3/2}D^{1/2}Cv^{1/2} \, [2]$$

234 where A is effective area of an electrode, n is electrons transferred number, D is the diffusion

235 coefficient, C is electrolyte solution concentration while v is the scan rate. The Cel CM/SPE had a

236 higher electroactive surface area by about 3 times in comparison with the Cel CM/SPCE (Fig. 3A).

237 The improvement in the electroactive surface of the Cel NFM/SPCE could be due to the unique

238 microporous structure of the nanofibrous membranes which can facilitate easy access of analytes

239 toward the surface of the electrode and accelerate the electron movement between the analyte and

240 the electrode surface, introducing the nanofibers as an ideal matrix for development of highly

241 sensitive sensing platforms.

242 Electrochemical impedance spectroscopy (EIS) is an effective technique for probing the features

243 of surface-modified electrodes made through the fabrication process. Impedance spectra consist of

244 two parts: a semicircle portion that corresponds to the electron-transfer-resistance (R_{et}), and a

245 linear portion which reflects the diffusion process [30]. Fig. 3B shows the Nyquist plots observed

246 after modification of the SPE surface with Cel NFM with different nanofibrous membranes

247 thicknesses of 0.05, 0.1 and 0.2 mm. It was shown that R_{et} was directly proportional to nanofibrous

248 membrane thickness. Due to its lower insulating effect, a membrane thickness of 0.05 mm was

249 found to be most suitable for further experiments.

250   Cyclic voltammograms were recorded with the developed immunosensor between −1 and 1 V vs

251   Ag/AgCl in PBS pH 7.2. No oxidation nor reduction peak was observed in the absence of AMN.

252   After incubation of the immunosensor with AMN at concentration of 1 µg mL^{-1}, one anodic peak

253   appeared at approximately 0.45 V, and a cathodic peak was observed at −0.05 V (Fig. 3C). The

254   anodic peak could be attributed to the electrochemical oxidation of AMN hydroxyindole to

255   quinone imine with two electrons and two protons. Based on these results, a potential of 0.45 V vs

256   Ag/ AgCl was selected for AMN immunosensing.
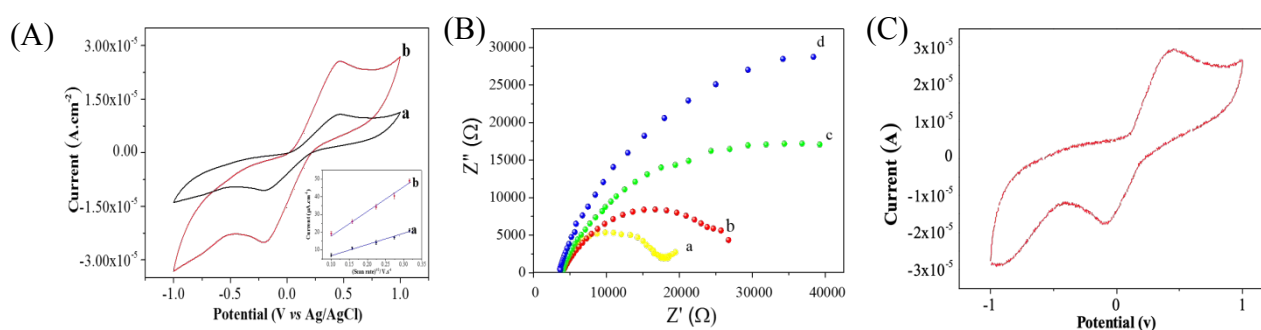
257
258   Fig.3. (A) CV of 2.5 mM [Fe(CN)^6]$^{3-/4-}$ at a scan rate of 25 mV s^{-1} for: (a) Cel CM/SPE and (b)
259   Cel NFM/SPE. (B) Nyquist plots of EIS in 2.5 mM [Fe(CN)^6]$^{4-/3-}$ for SPE surface modified with
260   (a) bare SPE, (b) Cel NFM (0.05 mm)/SPE, (c) Cel NFM (0.1 mm)/SPE, and (d) Cel NFM (0.2
261   mm)/SPE. (C) CV of AMN (1 µg mL^{-1}) on SPE.
262
263   ***Optimization of the experimental conditions for AMN detection***

264   The analytical performance of the fabricated immunosensor were adjusted by optimizing different

265   parameters including antibodies concentration, tethering time of antibodies, temperature and

266   immunoreaction time and the pH value of the electrolyte solution.

267

268   *Anti-AMN antibodies concentration*

269   The influence of antibody concentration on the sensor response to AMN (1 ng mL^{-1}) was examined

270   using the Cel NFM-modified SPE activated using 1mM EDC/NHS and an immobilization time of

271   60 min. The current response steadily increased as antibody loading increased. The highest

272   amperometric signal was achieved by using of anti-AMN antibodies at concentration of 100 μg

273   mL^{-1}. However, the sensor response was diminished at antibody concentrations greater than 150

274   μg mL^{-1} (Fig. 4a). This could be because of steric hindrance of the antibodies, which may influence

275   accessibility of the AMN molecules to the binding sites of the antibodies on the nanofibrous

276   membranes [31]. As a result, the ideal anti-AMN antibodies concentration for the immunosensor

277   fabrication was determined to be 100 μg mL^{-1}.

278

279   *Antibodies immobilization time*

280   By using the antibody immobilization procedure with antibodies concentration of 100 g mL^{-1} at

281   4°C for various durations ranging from 10 to 120 min, the impact of antibodies immobilization

282   time on the immunosensor response was investigated. The immunosensor response to AMN (1 ng

283   mL^{-1}) increased with raising the time of antibodies tethering up to 60 min Fig. 4b. Nonetheless,

284   longer incubation periods did not result in higher amperometric signals, indicating that active sites

285   on the nanofibrous membrane were saturated. Further experiments were carried out by using

286   immobilization time of 60 minutes.

287

288   *Immunoreaction temperature*

289   The AMN reaction with immobilized antibodies is significantly influenced by the incubation

290   temperature, which also affects the obtained current. The response signal was observed to raise

291   with increasing the temperature and reach a maximum value at 37 °C (Fig. 4c). Thereafter, the

292   signal progressively diminishes, most likely as a result of the denaturation of the immobilized

293   antibodies [32]. Therefore, 37°C was chosen as the ideal temperature for the formation of

294   immunocomplexes.

295

296   *Immunoreaction time*

297   The immunosensor response to AMN at the concentration of 1 ng mL^{-1} was assessed after

298   incubation durations varying from 5 to 60 minutes. Fig. 4d clearly indicates that the immunosensor

299   response raised linearly with incubation time and reaches a plateau after 30 minutes, showing that

300   the AMN molecules fully interacted with the immobilized antibodies [32].

301

302   *pH of the electrolyte solution*

303   The pH of the electrolyte solution is an important element in the performance evaluation of an

304   immunosensor. Fig. 4e depicts the influence of PBS pH values ranging from 5 to 8.5 on the current

305   response of the fabricated immunosensor. The experimental results demonstrated that the

306   immunosensor response increases as the pH value increases from 5 to 7.2, and subsequently

307   decreases as the pH value increases from 7.2 to 8.5. The reasons for this are most likely related to

308   the biological activity of the antibody, which decreased in acid and alkaline solutions, and the

309   antigen-antibody complex might readily disintegrate in the inappropriate pH of the working

310   solution [33,34].

311

312
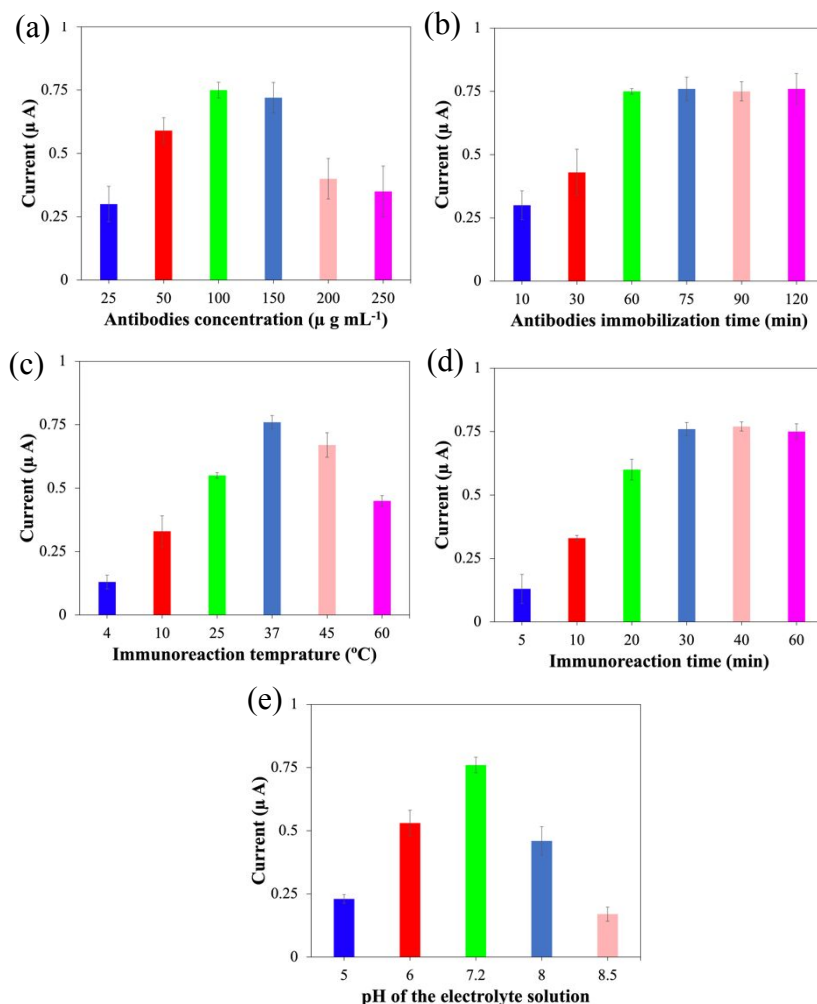
Fig.4. Response to 1 ng mL^{-1} AMN of immunosensors fabricated by using different experimental
conditions: (a) antibody concentration, (b) antibodies immobilization time, (c) immunoreaction
temperature, (d) immunoreaction time, (e) pH of electrolyte solution.

Detection of amanitin

With optimizing the different experimental factors, the analytical performance of the developed

immunosensor for AMN detection was investigated at different concentrations. A 100 µl of the

sample was added to the immunosensor surface and incubated at 37 °C for 30 min. After the

immunosensor washing with PBS buffer pH 7.2 to remove non-binded AMN, the electrochemical

measurements were carried out using PBS buffer (pH 7.2) as electrolyte. Figure 5A depicts the

324   DPV responses of the fabricated immunosensor at different concentration levels of AMN, it

325   was obvious that the achieved current increased as AMN concentration increased. As observed

326   in Figure 5B, the current responses exhibited a linear increase with the logarithm of AMN

327   concentration in the range of 9 pg mL^{-1} to 2 ng mL^{-1} (R^2=0.9901). The developed immunosensor

328   showed a high sensitivity toward AMN with a limit of detection (LOD) at 8.3 pg mL^{-1}

329   (LOD=3S$_b$ /m, where S$_b$ is the standard deviation of the blank and m is the slope of the calibration

330   plot.). The designed immunosensor performed good in terms of LOD and detection range, but

331   its key benefit is that direct detection of AMN and does not require any extra reagent. It is not

332   based on time-consuming and expensive AMN-conjugates-based competitive approaches. when

333   comparing the fabricated electrochemical immunosensor to other AMN detection biosensors

334   (Table 1), the developed nanofibers-based electrochemical immunosensor observed a good

335   behavior in terms of LOD and linear range with a main advantage is related to the fact that

336   detection of AMN is direct and does not involve any additional reagent. Moreover, the ultrahigh

337   sensitivity of the nanofibers-based electrochemical immunosensor could be attributed to

338   including the microporous nanofibrous membranes enhancing the accessibility of the AMN to

339   the recognition sites and accelerating the electron transfer, consequently improving the sensing

340   surface.

(a)

(b)
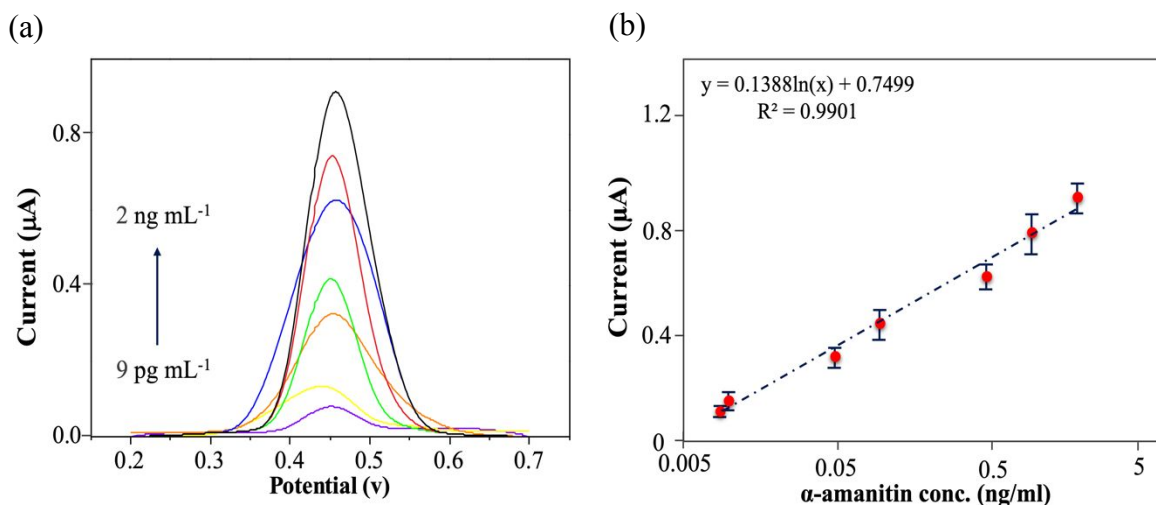
Fig. 5. (a) Electrocatalytic current responses of the fabricated electrochemical immunosensor for the detection of different concentrations of AMN in the range of 9 pg mL^{-1} to 2 ng mL^{-1}, (b) Calibration curve of the immunosensor for the detection of different concentrations of AMN. *(n=3)*

Table 1: Comparison of the detection ranges and detection limits of AMN of the developed immunosensor with other biosensors previously published researches.

Method	Range	LOD	ref
ELISA	1-6 µg/mL	0.1 µg/mL	[35]
LFIA	0.3-10 ng/mL	0.3 ng/mL	[36]
ELISA	1-120 ng/mL	0.91 ng/mL	[37]
LFIA	0.1-50 ng/g	0.1 ng/g	[38]
Fluorescent Aptasensor	0.01 - 5 µg/mL	7 ng/mL	[39]
ELISA	1.18-15.00 ng/mL	0.88 ng/mL	[40]
LFIA	0.3-10 ng/mL	0.3 ng/mL	[41]
Gold-nanoparticle based immunochromatographic	2 ng/mL- 2 µg/mL	1.9 ng/mL	[42]
Electrochemical immunosensor	0.009-2 ng /mL	8.3 pg /mL	This work

Immunosensor specificity, reusability, and stability

One of the main challenges in the field of sensing technology is developing a sensor to selectively

identify the desired target in samples comprising multiple closely related compounds. The

specificity of the fabricated immunosensor was studied by analyzing 0.1 ng mL^{-1} of mushroom

toxins including psilocybin, muscimol, and ibotenic acid as well as cyclic peptides including

microcystin-LR and nodularin. Cross reactivity (CR%) was investigated by calculating the

355   reaction to each antibiotic in terms of AMN-equivalent concentration using the AMN calibration

356   curve, it was presented as a percentage of AMN response [43]. As shown in Table S1, the developed

357   immunosensor was highly specific toward AMN as there was no cross-reactivity with all tested

358   compounds.

359   The ability of the fabricated immunosensor to be reused may help to lower the cost of medical

360   screening tests and minimize medical waste. After detecting 0.1 ng mL^{-1} of AMN, the fabricated

361   immunosensor was regenerate by dipping in 0.1M of glycine hydrochloric acid buffer at pH value

362   of 2.8 for 5 min. As shown in Fig. S1, the developed immunosensor demonstrated good reusability

363   by retaining more than 95% of its original activity after 4 assay cycles and around 88% after the

364   fifth cycle. The loss of activity might be brought either by denaturation of the immobilized

365   antibodies or destruction of the nanofibrous membranes during the repeated regeneration in an

366   acidic glycine buffer [34].

367   To investigate the stability, the immunosensor was kept at 4°C and its performance was checked

368   every week. After six weeks, the fabricated immunosensor demonstrated still good stability with

369   retaining more than 91% of its initial activity.

370

371   ***Applicability of the developed immunosensor***

372   To validate the feasibility of the fabricated immunosensor in the detection of AMN at low

373   concentrations in real samples, human urine samples were spiked with known concentrations of

374   AMN ranging from 0.01 to 1 ng mL^{-1}. Prior to spiking, the urine samples were analyzed using LC-

375   MS to confirm the free content of AMN. The spiked urine samples were diluted 2 times with PBS

376   without any further treatment before being examined blindly by the developed immunosensor.

377   Each concentration was tested in triplicate. As shown in Table 2, the recovery rate ranged from

378   92.9% to around 98.7%, with a relative standard deviation (RSD%) of about 4.8%. In addition to

379   the DPV responses of the fabricated immunosensor to different spiked urine samples (Fig. S2),

380   These aforementioned findings demonstrate the applicability, accuracy, and repeatability of the

381   fabricated immunosensor for rapid detection of AMN in the human urine at extremely lower

382   concentration without pre-cleaning for the samples.

383   **Table 2:** Recoveries of AMN from spiked human urine samples determined by the immunosensor.

Sample	Spiked concentration (ng mL^{-1})	Found concentration (ng mL^{-1})	Recovery (%)
1	0	ND	-
2	0.01	0.0093	92.9
3	0.05	0.0481	96.2
4	0.1	0.0943	94.3
5	1	0.987	98.7

384

385   **Conclusion**

386   An ultrasensitive, disposable, and rapid label-free electrochemical immunosensor for AMN

387   determination was successfully fabricated by using SPEs laminated with a layer of cellulose

388   nanofibrous membranes. The unique structure of cellulose nanofibrous membranes improved the

389   immunosensor response by about 3 times. The immunosensor showed very competitive analytical

390   performances with a LOD value of AMN at 8.3 pg mL^{-1}, as well as stability over time.

391   Furthermore, the feasibility of using the immunosensor in accurate determination of AMN in

392   human urine samples without any pretreatment has been demonstrated with good recovery during

393   around 30 min.

394

399

400   **References**

401   1   D. D. Gummin, J. B. Mowry, D. A. Spyker, D. E. Brooks, K. M. Osterthaler and W.
402   Banner, *Clin Toxicol*, 2018, **56**, 1213–1415.
403   2   W. E. Brandenburg and K. J. Ward, *Mycologia*, 2018, **110**, 637–641.
404   3   G. Cervellin, I. Comelli, G. Rastelli, F. Sanchis-Gomar, F. Negri, C. De Luca and G.
405   Lippi, *Hum Exp Toxicol*, 2018, **37**, 697–703.
406   4   K. A. Graeme, *Journal of Medical Toxicology*, 2014, **10**, 173–189.
407   5   F. C. Durand and D. Valla, *Drug-Induced Liver Disease*, 2013, 621–629.
408   6   S. L. Taylor, *Encyclopedia of Food Sciences and Nutrition*, 2003, 5813–5819.
409   7   C. S. Bever, K. D. Swanson, E. I. Hamelin, M. Filigenzi, R. H. Poppenga, J. Kaae, L. W.
410   Cheng and L. H. Stanker, *Toxins (Basel)*, 2020, **12**, 123.
411   8   T. P. Bambauer, L. Wagmann, A. A. Weber and M. R. Meyer, *Toxins (Basel)*, 2020, **12**,
412   1–14.
413   9   D. Varvenne, K. Retornaz, P. Metge, L. De Haro and P. Minodier, *Pediatr Emerg Care*,
414   2015, **31**, 277–278.
415   10   F. Enjalbert, S. Rapior, J. Nouguier-Soulé, S. Guillon, N. Amouroux and C. Cabot, *J
416   Toxicol Clin Toxicol*, 2002, **40**, 715–757.
417   11   C. Chen, X.-L. Zhao, Z.-H. Li, Z.-G. Zhu, S.-H. Qian and A. Flewitt, *Sensors*, 2017, **17**,
418   182.
419   12   G. A. Lopez, M.-C. Estevez, M. Soler and L. M. Lechuga, *Nanophotonics*, 2017, **6**, 123–
420   136.
421   13   A. Y. El-Moghazy, N. Wisuthiphaet, X. Yang, G. Sun and N. Nitin, *Food Control*, 2022,
422   **135**, 108811.
423   14   A. El-Moghazy, N. Amaly and G. Sun, in *29th Annual UC Davis Biotechnology Program
424   Retreat*, 29th Annual UC Davis Biotechnology Program Retreat, Davis, 2023.
425   15   A. El-Moghazy, N. Amaly and G. Sun, 2021, 8179.
426   16   J. Quirós, K. Boltes and R. Rosal, *Polymer Reviews*, 2016, **56**, 631–667.
427   17   S. S. Ray, S.-S. Chen, C.-W. Li, N. C. Nguyen and H. T. Nguyen, *RSC Adv*, 2016, **6**,
428   85495–85514.
429   18   X. Lu, C. Wang, F. Favier and N. Pinna, *Adv Energy Mater*, 2017, **7**, 1601301.
430   19   N. Amaly, P. Pandey, A. Y. EL-Moghazy, G. Sun and P. K. Pandey, *Talanta*, 2022, **242**,
431   123281.
432   20   N. Amaly, A. Y. EL-Moghazy, G. Sun and P. Pandey, *J Environ Manage*, ,
433   DOI:10.1016/j.jenvman.2020.111574.

434   21   A. Y. El-Moghazy, N. Amaly, G. Istamboulie, N. Nitin and G. Sun, *Microchimica Acta*,
435   2020, **187**, 535.
436   22   A. Y. El-Moghazy, J. Huo, N. Amaly, N. Vasylieva, B. D. Hammock and G. Sun, *ACS*
437   *Appl Mater Interfaces*, 2020, **12**, 6159–6168.
438   23   Q. Fu, Y. Si, C. Duan, Z. Yan, L. Liu, J. Yu and B. Ding, *Adv Funct Mater*, 2019, **29**, 1–
439   11.
440   24   H. Y. Liu H, *J Polym Sci—Polym Phys*, 2002, **40**, 2119–2129.
441   25   N. Amaly, Y. Si, Y. Chen, A. Y. El-Moghazy, C. Zhao, R. Zhang and G. Sun, *Colloids*
442   *Surf B Biointerfaces*, 2018, **170**, 588–595.
443   26   B. Cerroni, R. Cicconi, L. Oddo, M. Scimeca, R. Bonfiglio, R. Bernardini, G. Palmieri, F.
444   Domenici, E. Bonanno, M. Mattei and G. Paradossi, *Heliyon*, 2018, **4**, e00770.
445   27   Q. Fu, X. Wang, Y. Si, L. Liu, J. Yu and B. Ding, *ACS Appl Mater Interfaces*, 2016, **8**,
446   11819–11829.
447   28   S. S. B. Ding, C. Li, S. Fujita, *Colloid. Surface. A*, 2006, **285**, 257-262.
448   29   J. E. B. Randles, *Transactions of the Faraday Society*, 1948, **44**, 322–327.
449   30   F. J. Santaclara, R. I. Pérez-Martín and C. G. Sotelo, *Food Chem*, 2014, **143**, 22–26.
450   31   L. Qiao, X. Wang and X. Sun, *Int J Electrochem Sci*, 2014, **9**, 1399–1414.
451   32   N. Zhang, F. Xiao, J. Bai, Y. Lai, J. Hou, Y. Xian and L. Jin, *Talanta*, 2011, **87**, 100–105.
452   33   Y. Yang, Q. Liu, Y. Liu, J. Cui, H. Liu, P. Wang, Y. Li, L. Chen, Z. Zhao and Y. Dong,
453   *Biosens Bioelectron*, 2017, **90**, 31–38.
454   34   F. Li, J. Han, L. Jiang, Y. Wang, Y. Li, Y. Dong and Q. Wei, *Biosens Bioelectron*, 2015,
455   **68**, 626–632.
456   35   J. Gao, N. Liu, X. Zhang, E. Yang, Y. Song, J. Zhang and Q. Han, *Molecules*, ,
457   DOI:10.3390/molecules27020538.
458   36   C. S. Bever, K. D. Swanson, E. I. Hamelin, M. Filigenzi, R. H. Poppenga, J. Kaae, L. W.
459   Cheng and L. H. Stanker, *Toxins (Basel)*, , DOI:10.3390/toxins12020123.
460   37   K. He, Q. Mao, X. Zang, Y. Zhang, H. Li and D. Zhang, *Biologicals*, 2017, **49**, 57–61.
461   38   S. Zhou, L. Guo, X. Xu, S. Song, L. Liu, H. Kuang, Y. Zhu, L. Xu and C. Xu, *Food*
462   *Chem*, , DOI:10.1016/j.foodchem.2022.133660.
463   39   R. Tian, Y. Ye, X. Lu, J. Sun, W. Wang and X. Sun, *Highly Sensitive Fluorescent*
464   *Aptasensor for Detecting α-2 amatoxin Based on Rolling Circle Amplification Triggered*
465   *by Aptamer-Tetrahedral*, 2023.
466   40   H. Liu, Y. Qin, W. Xing and L. Ma, *Science and Technology of Food Industry*, 2022, **43**,
467   294–301.
468   41   C. S. Bever, C. A. Adams, R. M. Hnasko, L. W. Cheng and L. H. Stanker, *PLoS One*, ,
469   DOI:10.1371/journal.pone.0231781.
470   42   K. He, X. Zhang, R. Zhao, L. Wang, T. Feng and D. Wei, *Microchimica Acta*, 2016, **183**,
471   2211–2219.
472   43   V. Gaudin and P. Maris, *Food Agric Immunol*, 2010, 37–41.
473